Automatic thermograms segmentation, preliminary insight into Spilling Drop Test

by J. Melada*, P. Arosio**, M. Gargano** and N. Ludwig§**

* Dipartimento di Scienze della Terra "Ardito Desio", Università degli Studi di Milano, Via Cicognara 7, 20133 Milano, Italy
** Dipartimento di Fisica "Aldo Pontremoli", Università degli Studi di Milano, Via Celoria 16, 20133 Milano, Italy
§ corresponding author: Nicola.ludwig@unimi.it

Abstract

The Spilling Drop Test (SDT) is a non-destructive test that uses passive thermography to characterize the property of the building surfaces to absorb and diffuse water. However, the drops made visible by the evaporation process, show unclear contours that do not allow easy quantification of the wetted area. In this work, three image segmentation methods based on different statistical treatments have been considered in order to estimate the wet area. The information acquired by spilling drop test were also compared with standardized methods for the assessment of moisture in porous geomaterials. In addition, the pore size distribution was assessed by nuclear magnetic resonance. The proposed methods were tested by analyzing a set of ancient Roman plasters and modern mock-ups to highlight the ability of the thermographic method to provide useful information in the field of conservation of historical building materials.

1. Introduction

Thermographic techniques have always been widely used in historical and civil building surveys for the analysis of structures, but they can also be used for the in-situ evaluation of the properties of materials, in particular when dealing with issues related to the presence of water. Building materials consist mainly of porous systems with high surface-to-volume ratio [1]. Many properties of building materials such as mechanical strength, durability and moisture transport depend on porosity and on pore size distribution [2,3]. Recently, many studies for the determination of hygric properties of building materials [4] improved diagnostic methods and prevented damage and decay of façades or valuable surfaces (mosaic and frescoes) [5,6]. Nevertheless, porosity, and hydraulic properties such as sorptivity remain difficult to define due to the complexity of the phenomena involved in the liquid water-material interactions in plaster or stones [2,3]. Many standards in building science require relatively long measuring time and to have homogeneous materials both in shape and composition [3,4]. Moreover, the need for a certain amount of material usually demands invasive measurements through sampling or drilling. Recently, it was proposed to use the spilling drop test (SDT) to estimate the hygroscopic behaviour of materials surface or to evaluate the effectiveness of protective treatments [7-9]. The main advantages of this method are its non-invasiveness, the in situ applicability and the non-need for a priori knowledge of the homogeneity of the material. In the first experiment, a spilling drop acquisition consisted of 10 minutes of thermographic image capture of one drop of distilled water (3 μl) gently deposed on the horizontal surface of a material [9]. The thermal sequence displays the water spreading on the surface, according to the physical features of the material (Fig. 1). The temporal evolution of the wet area identifiable by IRT due to evaporative cooling, is the parameter which leads to an evaluation of the porosity and/or the surface microroughness of the material.
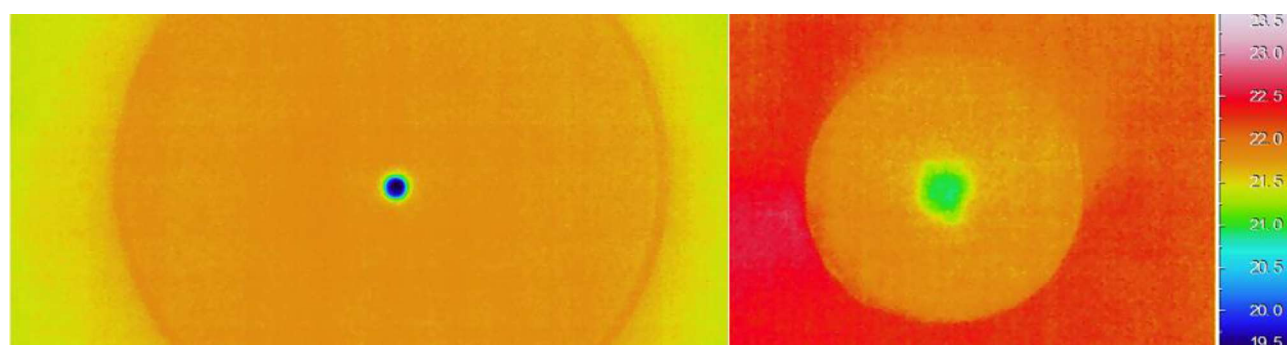

Figure 1. a.) water drop deposition on perfect non wettable surface (Teflon), b.) water diffusion on a core of brick, characterized by very high open porosity (images both recorded after 1 second of deposition, samples of different diameter), false color scale is in Celsius degrees.

Indeed, the rate of water spreading and the damp area was considered to depend mainly on the porosity of the material [8].

Two main problems arise when analysing the thermal image: first, the cooling measured on the surface of the sample is due to the effective diffusion of the water and not to the heat transfer. Figure 1a, drop on perfect non wettable surface, shows what happens when there is only heat transfer without water spreading, the green ring around the blue drop. The second is the difficulty in identifying precisely the limit reached by the expansion of the water due to the progressive weakening of the thermal contrast ($\Delta T = T_{dry} - T_{wet}$) between the wet and dry areas. The dynamic of wetting and heat transfer has been described by many authors [10,11] but though often on hydrophobic surface, or in the presence of high temperature difference in order to enhance the heat transfer or again by giving a kinetic energy to the droplet. The information obtained in this type of experiment positively affected our work, whose aim is to privilege the observation of the capillary diffusion of wettable surfaces. Therefore, we reduced both kinetic energy by acting a gentle deposition on the sample surface and keeping the difference of temperature between water and material in the range of 2-3°C.

The extent of penetration of spontaneous imbibition is known to increase with the square root of time following the Lucas-Washburn law [3,12]. However, in the case of expansion on a hemispherical volume starting from a single point-like quantity of liquid, it is possible to expect a different trend.

An important theoretical framework is presented, for example, in [13] when studying the influence of evaporation on the diffusion over the surface of thin layers of porous media, where, however, an unlimited reserve of water is considered. The model shows the equilibrium between evaporation loss and capillary penetration around the water source.

In this paper, the results of three automatic methods to measure the wet area are shown with the aim of obtaining a set of specific information about porous media in a non-invasive and automatic fashion. Thereby, one of the main purposes of this work is to select the best automatic algorithm for SDT data processing based on segmentation [14] and to evaluate its relationship with traditional standardized techniques [15] that characterize hydraulic properties of plasters.

The tests were also conducted on 2000 years old plasters, which represent the class of samples that cannot be tested invasively. Studies on this kind of materials represent an interdisciplinary field that connects archaeology, modern non-destructive techniques and civil building material characterizations [16]. Our preliminary results describe the latter as very resistant materials with a very low percentage of moisture spreading, possibly due to the high-level building technology reached by the Roman Civilization in the first centuries of the Christian era [17]. Another interesting field of application of this procedure of statistical analysis could be represented by electroosmotic drying devices of wet masonry, increasingly employed in heritage conservation despite the lack of a clear scientific base [18].

2. Materials and methods

The tests have been performed on mock-ups and on archaeological roman plaster samples (Table 1). Mock-ups were realized using putty-lime plaster, Portland cement and plaster with powdered bricks ("cocciopesto"). The archaeological samples come from a Roman site whose foundation dates back to the second half of the 2nd century BCE. Like all cultural heritage materials, these must be subjected to analyses that are as less destructive as possible. The reason for studying archaeological materials alongside laboratory mock-ups is to study the applicability of the SDT method also in real objects, far from the conditions of the tests subjected to regulations (UNI NORMAL [15]). In this work, the three selected samples were chosen as they are plaster monolayers carrying the various compositional differences found: pure cocciopesto plaster (RCp), painted cocciopesto plaster (RAr) and putty lime plaster (RMa).

2.1. Materials characterization

In order to characterize the materials of the samples utilized for the SDT (Table 1), the following properties were measured: moisture content (MC), open porosity (Φ), capillary absorption index (Acap), contact angle (α_w) and nuclear transverse relaxation times (T_2).

Table 1. Modern samples (M) and ancient roman plaster fragments (R) considered in this work.

Picture	Weight & description	Picture	Weight & description	Picture	Weight & description
	Mcp (15.36 g) Plaster with lime putty, natural micro-pozzolane, cocciopesto and calcareous/siliceous aggregates		**Mma (18.08 g)** Commercially available plaster consisting of lime putty and sand		**Mce (15.34 g)** Modern Portland cement and sand
MA2	**Rcpr (7.12 g)** Red ochre pictorial film on fine cocciopesto layer		**Rcp (3.76 g)** One layer of fine cocciopesto		**Rma (7.01 g)** One layer of lime putty plaster

The moisture content at saturation (MC) or imbibition capacity was determined by oven-dry gravimetry as recommended by many standards [15], i.e. the maximum amount of deionized water absorbed by a material for total immersion at environmental conditions. It is expressed as a percentage of the ratio of the mass of water inside the sample out of the mass of the dry sample. The mass of the dry sample and the mass of the saturated sample were measured using an electronic scale (10^{-4} g sensitivity).

The saturation or immersion technique determines the porosity of a material by saturating a sample with a liquid of known density and by calculating the pore volume from the weight difference between the fully saturated and dry condition. Deionized water was used as saturating fluid. Prior to saturation mock-ups and samples were kept in vacuum of about 5 k Pa for 6 hours in a vessel with silica gel, then they were saturated with deionized water under vacuum for one week. The weight of the saturated mock-ups and archaeological samples is determined after the excess of water is removed from their surfaces. The density of the saturating liquid and the open porosity was determined according to Kulia et al. [19].

The capillary absorption test, or water uptake test, determines the capillary absorption coefficient (Acap). It was measured according to the one-tanged method as described in [4]. The samples, which were previously oven-dried, were weighted every minute in order to measure the amount of water absorbed by capillary rising through the surface of samples in contact with deionized water. The same surface of the samples tested by SDT was used in order to evaluate Acap. All the aforementioned tests were performed after the samples were oven-dried for one night at 103° C in order to remove all free water in pores.

Contact angles were measured by deposition of a 10 μl drop of deionized water on 5 points of each dried samples surface. Images sequence of the drop have been acquired in the first 3 seconds by a Dino–Lite portable microscope with 35x magnification. The contact angle was measured with the ImageJ specific tool.

When performing broadband ^{1}H-NMR relaxometry measurements, the longitudinal nuclear relaxation time T_1 and the transverse nuclear relaxation time T_2, two parameters related to the relaxation process of the hydrogen nuclear magnetization, were measured. These parameters depend on the interaction between the hydrogen nuclei and the surrounding environment (i.e. other magnetic moments and all the other factors that interact with the spins of the hydrogen nuclei, like chemical functional groups, electron density, etc.). It must be noted that in the samples used for these measurements most hydrogen nuclei are water protons, therefore the obtained NMR signal reflects the information coming from the different water molecules inside the samples. In particular, NMR applied to saturated porous media measures the hydrogen nuclei concentration in the materials, which are imputed to fluids filling pore volumes [20]. Relaxation times of fluids confined in porous media are also strictly related to the geometry of the pores structure: the relaxation rate of water in porous media is increased in proportion to the surface-to-volume ratio (S/V) of the pore space [21]. Consequently, the ^{1}H-NMR measurements assuming a spherical shape of the pores can provide information on porosity and pore size distribution of the porous materials.

Before the acquisition of the measurements each sample was saturated according to the imbibition methodology described in paragraph 2.1.1. ^{1}H-NMR measurements were performed using a standard homemade broad-band spectrometer working at 25.15 MHz, corresponding to a magnetic field of 0.59 Tesla. The coil was designed to adapt perfectly to dimension of samples, in order to maximize the filling factor and, consequently, to increase the signal-to-noise ratio and thus to perform fast measurements. Both longitudinal (T_1) and transverse (T_2) relaxation times were acquired using standard pulse sequences, namely a saturation recovery for T_1 measurements and a Carr–Purcell–Meiboom–Gill (CPMG) for T_2 measurements (pulse: $\pi/2$ = 2.5 µs, repetition time: RT = 2 s). In this paper only the results obtained for T_2 measurements are presented. The echo time for the CPMG sequence was set to 100 µs and the maximum number of accumulated scans was set to 100 for each sequence. The echo signal integrated over time has been plotted as a function of different delay times, as usual in the T_2-decay curve, and it has been observed the multiexponentiality of the curves of all the samples analysed. Therefore, using the Uniform PENalty (UPEN) inversion algorithm that performs the inverse Laplace transform on multi-exponential relaxation curves, the T_2 distribution has been obtained. The UPEN results have been also compared with a fitting model of the experimental curves, that implements the sum of different exponential decays (up to 5 components), by means of Microcal Origin software.

2.2. Spilling drop test

The thermograms sequences were acquired using the FLIR A65 thermographic camera (long wave microbolometric, 30 Hz, NETD < 0.05 K @ room temperature) placed at a constant distance of 16 cm from the horizontal surface. The water drop (3 µl) at a temperature of about 20°C was poured onto the materials by means of a micropipette avoiding any fall (Fig. 1). SDT has been carried out using two intervals of data acquisition and 3 different image processing algorithms. In this work an important new step was added to the procedure already described in the previous work [9], increasing the frequency of acquisition in the first few seconds after the drop deposition. This novelty is of fundamental importance considering the fast interaction phenomena in water absorption. Image acquisition was made for 30 s @ 10 Hz in order to reach a trade-off between amount of acquired data, time of the analysis and computational processing cost. All the work was carried out at a room temperature of 22 ± 2 °C and a relative humidity of 54 ± 3%. The little temperature difference between drop and plaster has been considered sufficient to enhance the thermal signal of the wet area but not relevant to cause a considerable heat transfer which could affect the correct reading of the evaporating area. The

experiment was repeated 5 times for each sample for a total amount of 30 drops on the six plaster samples of table 1 which differ for materials, ageing and constructive techniques.

The problem of the exact determination of the extent of moistened areas in passive thermography with segmentation techniques has been extensively studied by authors dealing with moisture diffusion [22] as well as the problem of the use of authomatic pre-processing algoritms on building inspection [23]. In spilling drop test, on the other hand, the quantity of water is very limited compared to that involved in capillary rise and the concentration of water in the pores decreases in seconds. The temperature matrix of the thermograms were first cropped around the drop in order to obtain a 100x100 pixel image and they were subsequently converted to 8-bit grayscale. The images were denoised preserving the edges using a bilateral gaussian filter [13]. The drop was then automatically segmented exploiting 3 different automatic thresholding algorithms: Otsu's method [24], Li's method [25] and Yen's method [26] in order to extract the area of the drop from images and represent it proficiently. The thresholding methods were compared according to a busyness criterion first suggested in [27] using the co-occurrence matrix of the grayscale image. In fact, it is assumed that the drop would present a simple compact non-textured shape during the spreading until its evaporation or absorption by the material itself. A region nonuniformity measure was also computed as an additional indication of the performance of the segmentation algorithm [28]. The area of each drop was calculated for all the thermographic sequences using the mentioned three thresholding algorithms. The pattern of each drop in time was extracted and the data filtered with a moving average filter with 15 data points window size in order to remove the noise. In order to avoid fluctuations due to thermal instability, such as microbolometric drift, the results show a relative increase with respect to the initial value of the drop area.

Finally, as we are dealing with surfaces that show different composition, some consideration on emissivity are included. Water emissivity (0.95-0.96) in long wave range overcomes that of most building geo-material such as mortar, brick powder, concrete, sand (0.70-0.88) [29], and at room temperature this difference is compensated by reflection of the environmental radiation. In order to avoid any additional and more relevant influence of absorption of near-infrared radiation we reduced this radiation with the use of fluorescent lamps.

3   Results

3.1   Materials characterization

Sample	MC (%)	Φ (%)	α_w (deg)	A_{cap} (Kg·m^{-2}·s$^{-0.5}$)
Mcp	26.81	41.64	49.1	0.31
Mma	20.62	35.62	35.0	0.28
Mce	21.33	36.12	28.5	0.31
Rcpr	32.31	40.32	36.3	1.16
Rcp	24.33	39.43	36.0	0.36
Rma	21.86	36.28	93.3	0.47

Table 2. Sample hydraulic properties: moisture content (MC), open porosity Φ, contact angle α_w and capillary absorption (A_{cap}). Extreme values are underlined.

Table 2 and figure 2 resume the main important characteristics that can affect water diffusion and consequentlty SDT measurements. The differences in MC and open porosity for cocciopesto based plaster samples testify the exceptional hydraulic properties of ancient roman plaster made in cocciopesto and the abnormous Acap value of the Rcpr sample due to the painted layer but also to the peculiar pore size distribution found by NMR relaxation measurements.
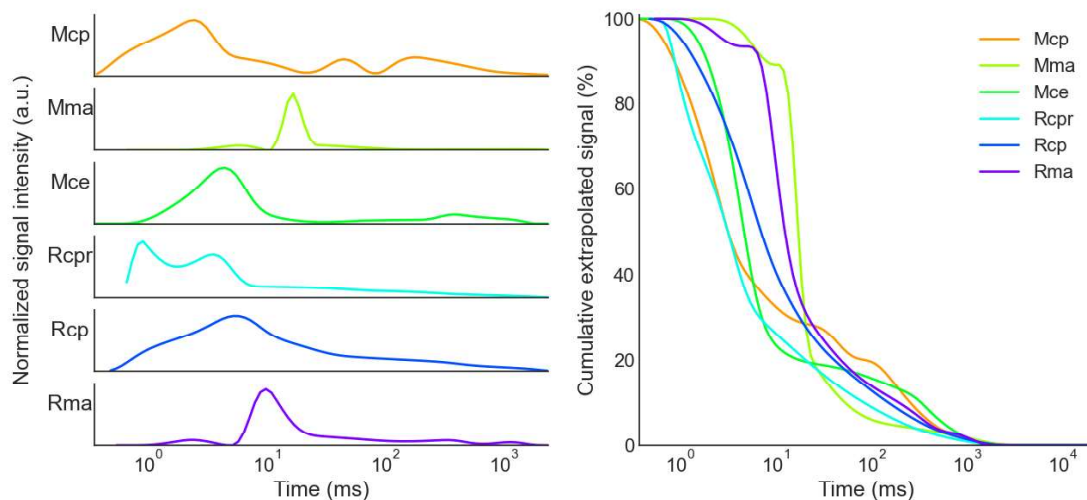
Figure 2. ^{1}H-NMR relaxometric results. On the right: cumulative signals of the samples clearly show their differences and, in particular, that Rma and Mma are characterized by a poor loss of signal till 8-10 ms, followed by its deep decrease and a smooth decrease of the remaining part. On the left: inverted nuclear relaxation time distributions obtained by Upen. The correlation between signal (right) and nuclear time distributions (left) is evident, indeed the curves of distribution clearly differentiate all the samples. E.g. the poor loss of the signals for Rma and Mma at short times correspond to the substantially absence of times (and consequently pores of small dimensions, see the text) below 8 ms.

For what concerns ^{1}H-NMR relaxometry, it must be mentioned that it is a technique able to follow the hydrogen nuclear magnetization relaxation processes. In figure 2 the cumulative signals of the nuclear relaxation decay curves of all samples, on the right, and the correlated nuclear time distributions obtained by Upen, on the left, are shown. As can be evinced by the decay curves in the time domain, the materials could be immediately differentiated from each other and the multiexponentiality of the curves indicates that several components contribute to the nuclear relaxation. In other terms the technique is sensitive to different "class of hydrogen nuclei" that are present in the samples. Considering that the predominance of the hydrogen nuclei in the measured samples is constituted by the protons of the water molecules, the obtained signals are mostly due to the water molecules used to saturate the samples. For this reason, the ^{1}H-NMR are useful to extract information on the porosimetry of the materials, since the saturation water molecules filled the pores. In details, the protons in pores of different size contribute in a different way to the nuclear relaxations, because the magnetic interactions between the nuclear spins of the nuclei and between them and the lattice change in function of the dimension of the pores. Indeed, the protons in small pores are obliged to interact more each other and with the lattice compared to the larger pores situation, which means that those protons relax faster and contribute to the overall NMR signal in the first part of time domain. Processing the experimental signals by means of the inverse Laplace transform using Upen algorithm, the multi exponential curves were inverted and the obtained distributions of relaxation times are correlated to the pore size distribution. The Mma, Mce and Rma samples, although with broader or narrower distributions, are substantially characterized by one class of T2 times or in other word one class of water protons, which in turn corresponds to one single class of pore size in the samples. The other 3 samples, on the contrary, showed the co-presence of a certain number of pore sizes classes, as can be seen in Rcpr sample, where two classes are evident, going all the way to the more complexes cases of Mcp and Rcp.

3.2   Drop spread evaluation by thermography

Water diffusion in porous geo-materials (stones, plaster, bricks…) is driven by capillarity force and the water front speed is well described by the Lucas-Washburn law in a horizontal experimental set-up when gravity can be neglected. As much as heat diffusion, capillary diffusion depends on the square root of time through a parameter, the sorptivity, that is used to express the capacity of the materials to transport and absorb water and whose determination without sampling can be extremely useful for surface characterization of monuments.

On the samples examined in this work the area soaked by the drop is clearly visible in thermography both for the different initial temperature of the water and thanks to the evaporation which keeps the soaked areas colder even when the water is dispersed within the capillary network of the material, an example can be seen in Fig 3.
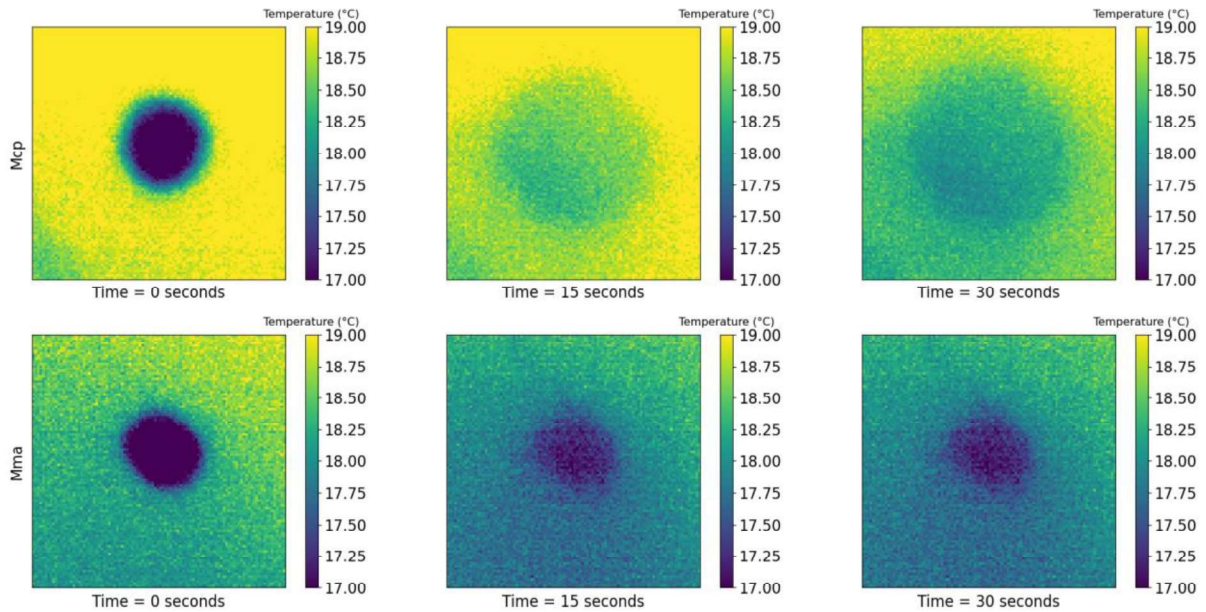
Figure 3. Water drop spreading on two samples surfaces (Mcp and Mma) at different time.

The contrast between the surface temperature of the wet and surrounding dry material becomes negligible after a few seconds and it is no longer possible to distinguish the wet area (Fig. 4), this value with us experimental set up is around 0.5°C. Thermal contrast exhibits the same decay over time for all samples and all segmentation algorithms. Initially, the thermal contrast between the drop and the dry surface of the materials settles around 2 °C and then drops below 0.5 °C after the first 10 seconds. However, it can be noted that for the Mma and Rma samples the thermal contrast remains slightly higher in the first half of the curve. From this assumption we will focus on the first 10 seconds for subsequent analysis.
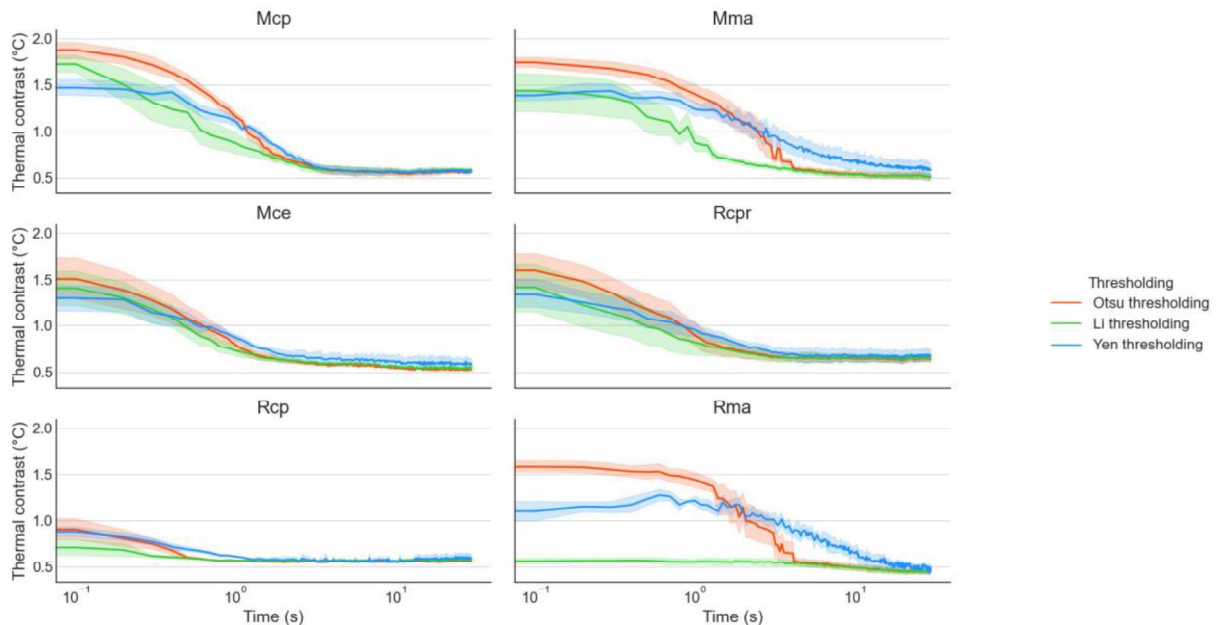

Figure 4. Temperature contrast between the foreground object (drop) and the background object (dry material) as mapped by the three thresholding methods. Average values of 5 drops for each sample.

In the cited previous work the thermogram at maximum wet area extension (visually identified by the operator) was used to characterize the materials through the relative increase of the wet area with respect to the moment of the drop deposition [8, 9]. The wet areas were calculated approximating them with a circle having diameter equal to the of colder

temperature (i.e. maximum thermal gradient along a profile crossing the sample). In this work we propose a method to automatically obtain the pattern of the drop area using consolidated segmentation algorithms. By doing so, we considered the drop size vs time relation.

During the first 30 seconds after the drop deposition, the drop area increases (Fig. 3) driven by chemical and mineralogical composition of the samples that influence the surface hydrophilicity, and by the pores network characteristics (amount, radius, dimensional distribution and shape). Meanwhile the thermal contrast diminishes gradually (Fig. 4) making more difficult the segmentation of the considered area. The histogram of the grayscale images (Fig. 5, second row) changes in time increasing the difficulty in finding the boundary of the drop due the loss in thermal contrast between wet and dry areas. In the third row of the same figure are shown the results for the different methods of automatic segmentation considered: Otsu, Li and Yen. In figure 5 it is possible to compare the main differences in their operating principles in a single drop case.
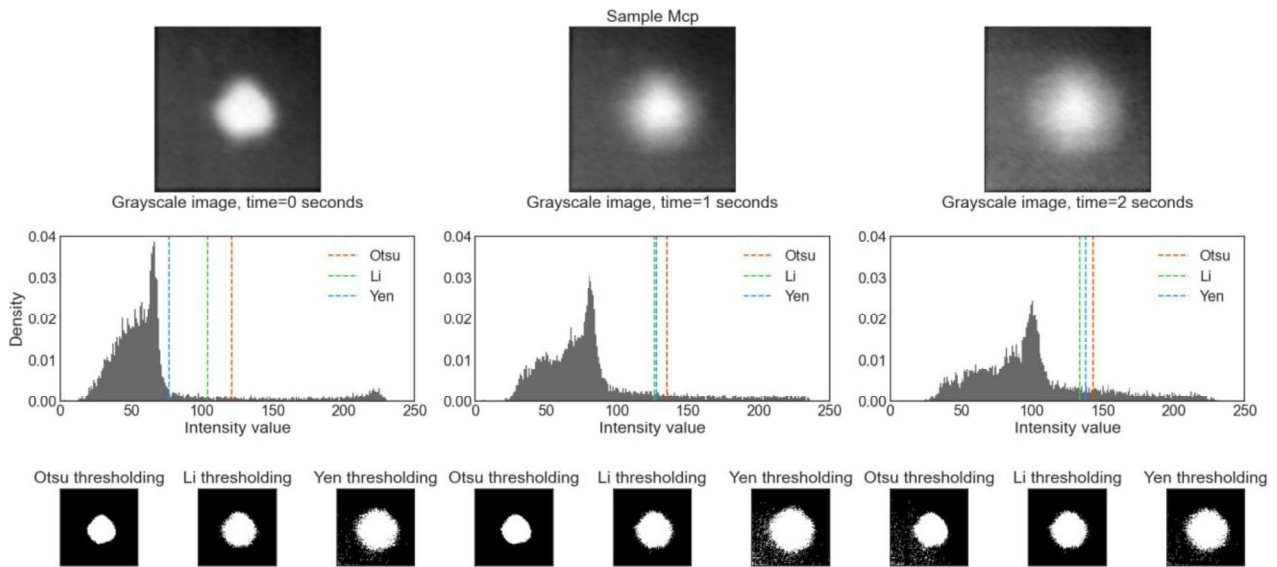

Figure 5. Example of automatic thresholding by the three methods (Otsu, Li and Yen) to obtain the segmentation of the wet area at different times.

For the Mcp sample the three curves (see Fig. 6) show more or less the same trend with a certain time shift. On the other hand, for the roman sample the growth curves of the drop area appear very different: for the segmentation obtained by the Otsu method it grows rapidly during the first 5 seconds and then it continues to grow in a less steep way, while the curves obtained with segmentation Li and Yen show a drop that does not expand over time.

Since there are no ground truth measurements for the area all the thresholding algorithms are considered for further data analysis and compared using the busyness criterion and the region non-uniformity index as indications for the quality/validity of the obtained segmentation. The busyness index was calculated for each grayscale image summing the co-occurrence matrix's entries that represent the percentage of object-background adjacencies. Comparing the distributions of the busyness index, a higher busyness index would suggest a large amount of noise or areas with jagged edges. Fig. 6 shows the busyness index distribution calculated for all the time sequences, all the samples and all the thresholding algorithms. As can be seen, all the methods in our study show a similar amount of busyness in images that present all the interquartile range below 10 units of busyness with few exceptions. Nevertheless, Yen's method seems to perform a better segmentation. This observation is slightly supported by the region non-uniformity measure (Fig. 7) and will be discussed in the following section 3.3 in comparison with the sample physical characteristics of table 2 and NMR results.
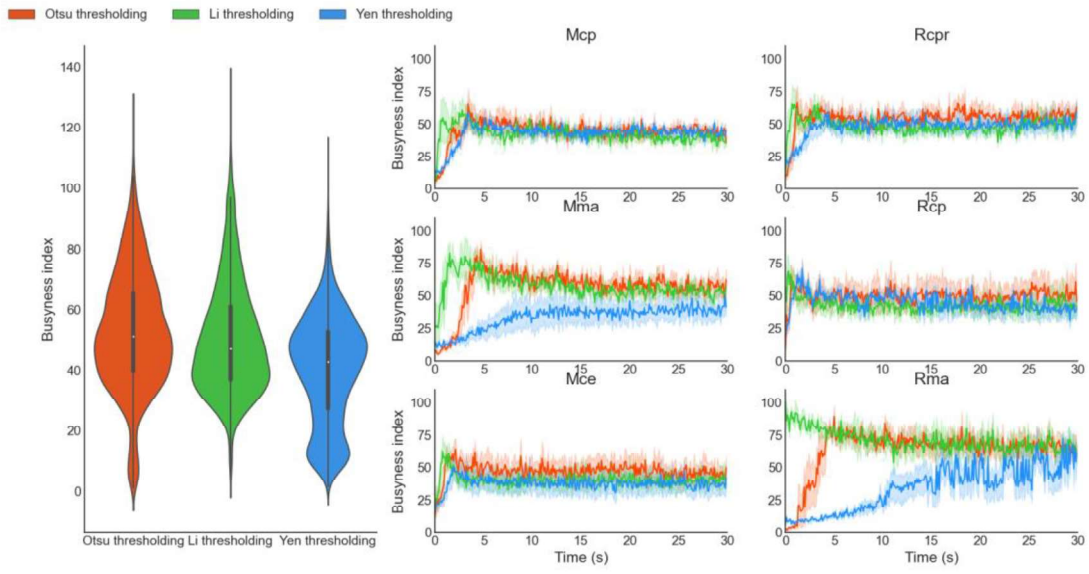
Figure 6. Left, busyness index distribution for all three thresholding algorithms; right, the time sequences for each sample. The white dot in diagram on the left is the representation of the mean value of the busyness index frequency distribution, Yen method shows the lowest.
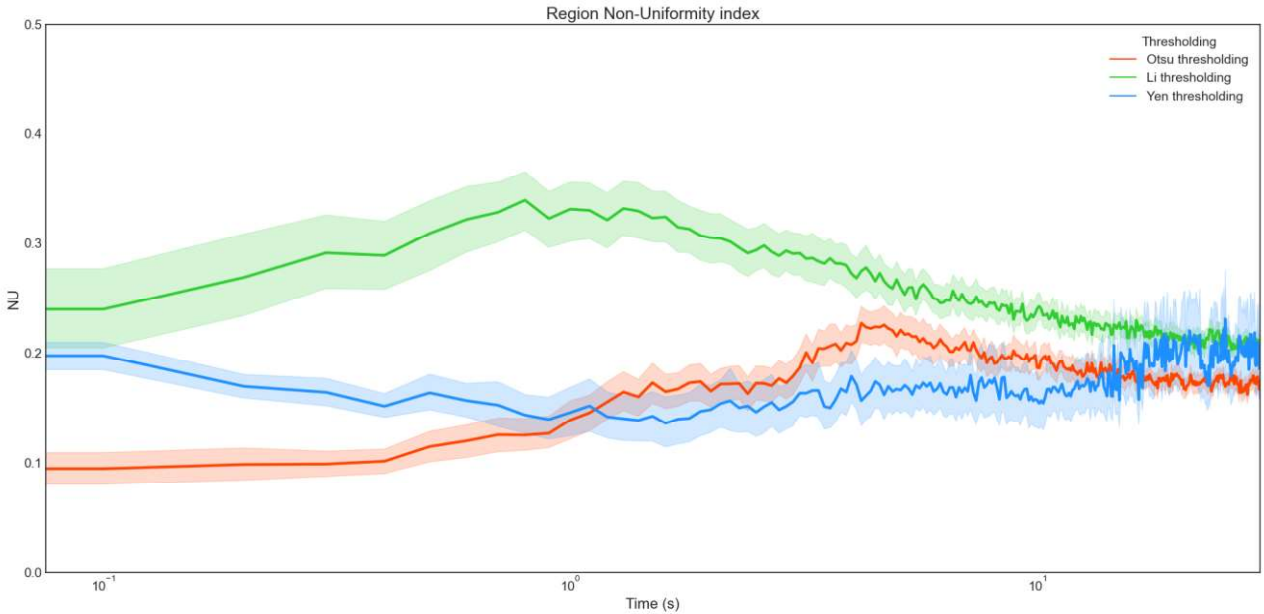

Figure 7. Region non-uniformity index along all the acquisition time (Log scale). The data are grouped by thresholding algorithm in order to compare their performance on all samples. The shadow areas represent the interquartile range.

3.3 Comparison of segmentation methods

The drop's area evolution was calculated using different algorithms and has been expressed as the ratio of the spread drop area against its initial value. To classify the obtained curves, we observed the values up to 10 seconds and estimated the tendency of the three algorithms (Fig. 8), after which the values become constant. As a first attempt we can single out 3 classes: class A includes those materials whose relative increase in the drop area at 10 seconds is <100%. In this case the material is not very absorbent, and the water does not spread. Yen's method identifies Mma and Rma samples that show a similar trend in the area increase. Class B includes materials with a relative increase ranging between 100%

and 300%. These are materials on which the drop expands up to threefold. Finally, class C includes all the materials on which the drop increases more than 3 times from the initial area. While the Otsu method seems to be unable to distinguish these three classes as it assigns enormous expansion values to all the considered samples, the Li method equally distributes the six over the whole span of percentage increase.

Furthermore, comparing the SDT results with the gravimetric ones (Table 2) is difficult as it lacks enough statistics even if Yen method singles out the same two samples with the largest relaxometric times (Rma and Mma). It can be therefore confirmed that the spilling drop is not an optimal method to obtain information about the capillary absorption or the porosity of the materials as it typically provides only superficial and non-volumetric indications, unlike the other hygroscopic parameters. At this stage the segmentation tests studied and in particular the Yen one shows the possibility of using infrared thermography to estimate the wettability or surface roughness of the materials and the capillary network in the very superficial layer where the most important interactions and water/energy exchanges between geo-material and air occur.
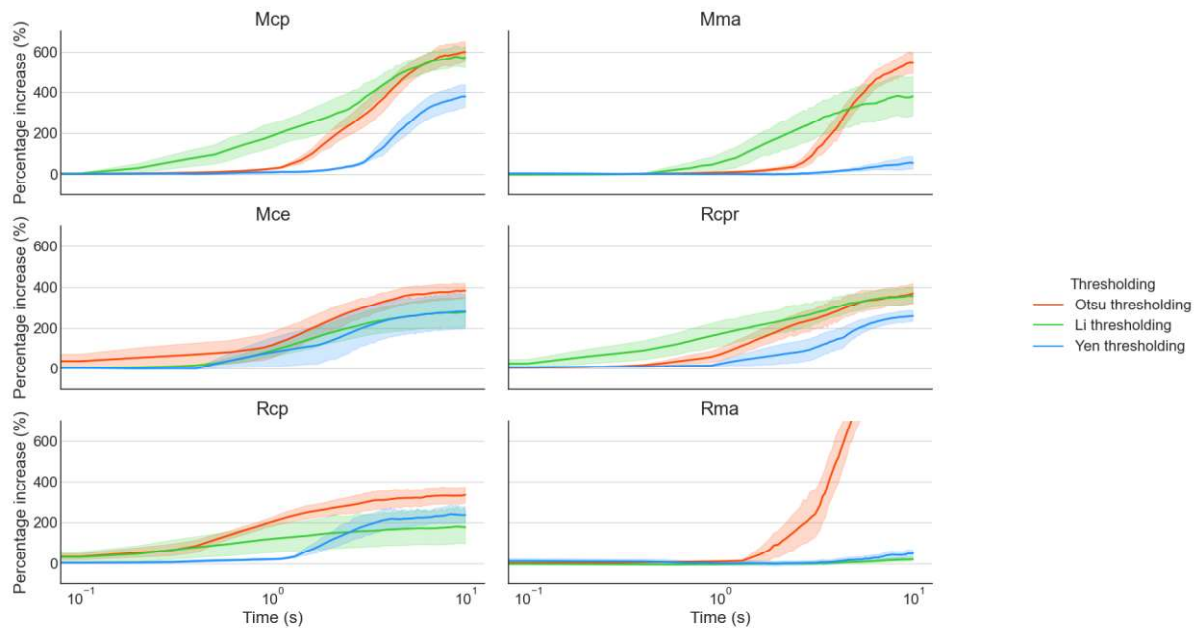

Figure 8. Percentage increase of the drop areas during the first 10 seconds (Log scale). The shadow areas represent the interquartile range.

4 Conclusions

This work investigates new non-invasive thermography based methods to study building materials, it opens new interesting future perspectives in three main fields: the physics of mass-energy transport inside a porous medium, the automatized segmentation in noisy thermal images and the issues of Cultural Heritage conservation in moist environments. The aim of this paper is to better define time and experimental conditions of spilling drop test, and to add useful case-studies in the in the field of area segmentation, particularly interesting when dealing with passive detection of water in walls. Furthermore, the SDT has been tested here on historical plaster, in order to estimate their hygroscopic characteristic in non-invasive ways.

The spilling drop test has proved to detect different behaviour of water spreading in building materials such as plaster. Our test demonstrates that the first 10 seconds and a high sampling rate (30 Hz) are the most important parameters to allow a classification of the materials due to both the rapidity in capillary suction and the duration of the evaporation cooling. After the first 10 seconds the percentage increase of the area tends to be similar for all the methods thus suggesting that segmentation algorithms simply separate between cold and warm pixels, without taking into account the circular shape of the drop.

In conclusion, this work shows the differences between three segmentation methods to calculate the area in an automated way. As partially predictable, no direct correlation was found between volume properties such as porosity obtained by imbibition and magnetic reflectometry measurements with NMR. On the contrary, the area measurements show a significant agreement with the surface hydraulic properties in terms of contact angle and capillary absorption. As regards the use of segmentation algorithms an important result is that the differences in the materials properties are found already in the initial stages when the thermal contrast is stronger and the area of the drop is easier to identify. An important

further step could be to experiment the use of image segmentation algorithms based on iterative region growing [14] as suggested for biomedical applications.

In the future, an interesting line of application of the SDT method tested so far is the study of biofilms, whose role in the conservation/deterioration of stone surfaces is the subject of debate [30]. The SDT could evaluate the abrupt change of hydraulic properties due to the implantation of colonies of bacteria.

REFERENCES

[1] Brai, M., Casieri C., De Luca F., Fantazzini P., Gombia M., Terenzi, C., Validity of NMR pore-size analysis of cultural heritage ancient building materials containing magnetic impurities. *Solid state nuclear magnetic resonance*, vol. 32(4), pp. 129-135, 2007.

[2] Anovitz, L. M., Cole D. R., Characterization and analysis of porosity and pore structures. *Reviews in Mineralogy and geochemistry* vol. 80.1, pp. 61-164, 2015

[3] C. Hall, W.D. Hoff, Water transport in brick, stone, and concrete. (3rd edition2021), CRC press. *https://doi.org/10.1201/9780429352744*

[4] Feng, C., Janssen H., Feng Y., Meng Q, "Hygric properties of porous building materials: Analysis of measurement repeatability and reproducibility". *Building and Environment,* vol. 85, pp. 160-172, 2015.

[5] Melada, J., Arosio, P., Gargano, M., Veronese, I., Gallo, S., & Ludwig, N. (2020). Optical reflectance apparatus for moisture content determination in porous media. *Microchemical Journal, 154*, 104627.

[6] Capineri, L., Capitani, D., Casellato, U., Faroldi, P., Grinzato, E., Ludwig, N., (2011). Limits and advantages of different techniques for testing moisture content in masonry. *Materials Evaluation*, 69(1), 111-116.

[7] Rosina, E., Ludwig, N., Torre, S. D., D'Ascola, S., Sotgia, C., & Cornale, P. (2008). Thermal and hygroscopic characteristics of restored plasters with different surface textures. *Materials evaluation*, 66(12), 1271-1278.

[8] Sansonetti, A., Casati, M., Rosina, E., Gerenzani, F., Gondola, M., & Ludwig, N. (2012). Contribution of IR thermography to the performance evaluation of water repellent treatments. *Restoration of Buildings and Monuments*,18(1), 13-22

[9] Ludwig, N., Rosina, E., Sansonetti, A., Evaluation and monitoring of water diffusion into stone porous materials by means of innovative IR thermography techniques. *Measurement,* vol. 118, pp. 348-353, 2018

[10] Qi, W., & Weisensee, P. B. (2020). Dynamic wetting and heat transfer during droplet impact on bi-phobic wettability-patterned surfaces. *Physics of Fluids*, 32(6), 067110.

[11] Schmidt, J. B., Breitenbach, J., Roisman, I. V., & Tropea, C. (2018, November). Measurement of the Heat Flux During a Drop Impact onto a Hot Dry Solid Surface Using Infrared Thermal Imaging. In *Symposium der Deutsche Gesellschaft für Luft-und Raumfahrt* (pp. 553-562). Springer, Cham.

[12] Li, K., Zhang, D., Bian, H., Meng, C., & Yang, Y. (2015). Criteria for applying the Lucas-Washburn law. *Scientific reports*, 5(1), 1-7.

[13] Liu, M.; et al. (2016). Evaporation limited radial capillary penetration in porous media. *Langmuir*.**32** (38): 9899–9904. doi:10.1021/acs.langmuir.6b02404

[14] Hakim, A. S., & Awale, R. N. (2022). Extraction of hottest blood vessels from breast thermograms using state-of-the-art image segmentation methods. Quantitative InfraRed Thermography Journal, 1-19(5), 347-365.

[15] EN 16682 Conservation of Cultural Heritage – Methods of Measurement of Moisture Content, or Water Content, in *Materials Constituting Immovable Cultural Heritage European Committee for Standardization (CEN),* Brussels (2017)

[16] Bartz, W., Rogóż, J., Rogal, R., Cupa, A., & Szroeder, P. (2012). Characterization of historical lime plasters by combined non-destructive and destructive tests: The case of the sgraffito in Bożnów (SW Poland). *Construction and Building Materials*, 30, 439-446.

[17] Al-Bashaireh, K. S. .Chronology and technological production styles of Nabatean and Roman plasters and mortars at Petra (Jordan). Phd dissertation of Khaled Shenwan Al-Bashaireh,The University of Arizona ProQuest Dissertations Publishing, 2008. 3315952.

[18] Melada, J., Gargano, M., Veronese, I., & Ludwig, N. (2018). Does electro-osmosis work in moisture damage prevention? Applicability of infrared-based methods to verify water distribution under electric fields. *Journal of Cultural Heritage*, 31, S38-S45.

[19] Kuila, U., McCarty, D.K., Derkowski, A., Fischer, T.B., Prasad, M., Total porosity measurement in gas shales by the water immersion porosimetry (WIP) method, *Fuel.* 117 (2014) 1115–1129

[20] Olatinsu, O. B., Olorode, D. O., Clennell, B., Esteban, L., & Josh, M. (2017). Lithotype characterizations by Nuclear Magnetic Resonance (NMR): a case study on limestone and associated rocks from the eastern Dahomey Basin, *Nigeria.Journal of African Earth Sciences*,129, 701-712.

[21] Fantazzini, P. (2005). Magnetic resonance for fluids in porous media at the University of Bologna. *Magnetic resonance imaging,* 23(2), 125-131..

[22] Garrido, I., Lagüela, S., Sfarra, S., Madruga, F. J., & Arias, P. (2019). Automatic detection of moistures in different construction materials from thermographic images. *Journal of Thermal Analysis and Calorimetry*, 138(2), 1649-1668.

[23] Garrido, I., Lagüela, S., Fang, Q., & Arias, P. (2022). Introduction of the combination of thermal fundamentals and Deep Learning for the automatic thermographic inspection of thermal bridges and water-related problems in infrastructures. *Quantitative InfraRed Thermography Journal*, 1-25.

[24] Xu, X., Xu, S., Jin, L., & Song, E. (2011). Characteristic analysis of Otsu threshold and its applications. *Pattern recognition letters,* 32(7), 956-961.],

[25] Li, C. H., & Tam, P. K. S. (1998), An iterative algorithm for minimum cross entropy thresholding. *Pattern recognition letters*, 19(8), 771-776.]

[26] Yen, J. C., Chang, F. J., & Chang, S. (1995). A new criterion for automatic multilevel thresholding. *IEEE Transactions on Image Processing*, 4(3), 370-378.

[27] Weszka, J. S., & Rosenfeld, A. (1978). Threshold evaluation techniques. *IEEE Transactions on systems, man, and cybernetics*, 8(8), 622-629.

[28] Sezgin, Mehmet, and Bülent Sankur. Survey over image thresholding techniques and quantitative performance evaluation. Journal of Electronic imaging 13.1 (2004): 146-165.

[29] Avdelidis, N.P., Moropoulou, A., Emissivity considerations in building thermography, Energy and Buildings, Vol 35, 7, 2003, 663-667, ISSN 0378-7788, doi.org/10.1016/S0378-7788(02)00210-4.

[30] Villa, F., Ludwig, N., Mazzini, S., Scaglioni, L., Fuchs, A. L., Tripet, B., ... & Cappitelli, F. (2023). A desiccated dual-species subaerial biofilm reprograms its metabolism and affects water dynamics in limestone. *Science of The Total Environment*, 161666.